AGU PUBLICATIONS

JGR

Journal of Geophysical Research: Earth Surface

RESEARCH ARTICLE
10.1002/2016JF003953

Key Points:
- Direct measurements of bedrock fault surface exposure in the central Apennines
- Registered exposure occurred without contributing tectonic/seismogenic movement
- Fault slip rates and earthquake recurrence periods calculated from only bedrock fault surface exposure are called into question

Supporting Information:
- Supporting Information S1

Correspondence to:
V. Kastelic,
vanja.kastelic@ingv.it

Citation:
Kastelic, V., P. Burrato, M. M. C. Carafa, and R. Basili (2017), Repeated surveys reveal nontectonic exposure of supposedly active normal faults in the central Apennines, Italy, *J. Geophys. Res. Earth Surf.*, *122*, 114–129, doi:10.1002/2016JF003953.

Received 10 MAY 2016
Accepted 13 DEC 2016
Accepted article online 15 DEC 2016
Published online 11 JAN 2017

Repeated surveys reveal nontectonic exposure of supposedly active normal faults in the central Apennines, Italy

Vanja Kastelic[1], Pierfrancesco Burrato[2], Michele M. C. Carafa[1], and Roberto Basili[2]

[1]Istituto Nazionale di Geofisica e Vulcanologia, L'Aquila, Italy, [2]Istituto Nazionale di Geofisica e Vulcanologia, Rome, Italy

Abstract We investigate the geomorphic processes that expose bedrock fault surfaces from under their slope-deposit cover in the central Apennines (Italy). These bedrock fault surfaces are generally located at various heights on mountain fronts above the local base level of glacio-fluvial valleys and intermountain fluvio-lacustrine basins and are laterally confined to the extent of related mountain fronts. The process that led to the exposure of fault surfaces has often been exclusively attributed to coseismic earthquake slip and used as proxy for tectonic slip rates and earthquake recurrence estimations. We present the results of monitoring the contact between the exposed fault surfaces and slope deposits at 23 measurement points on 12 different faults over 3.4 year long observation period. We detected either downward or upward movements of the slope deposit with respect to the fault surface between consecutive measurements. During the entire observation period all points, except one, registered a net downward movement in the 2.9–25.6 mm/yr range, resulting in the progressive exposure of the fault surface. During the monitoring period no major earthquakes occurred in the region, demonstrating that the measured exposure process is disconnected from seismic activity. Our results indicate that the fault surface exposure rates are rather due to gravitational and landsliding movements aided by weathering and slope degradation processes. The so far neglected slope degradation and other (sub)surface processes should thus be carefully taken into consideration before attempting to recover fault slip rates using surface gathered data.

1. Introduction

The central Apennines (Italy) are a mountain chain affected by postcollisional active extension along NW-SE striking normal faults, known since the work of *Elter et al*. [1975], and well-documented regional-scale uplift. The normal faults affect Meso-Cenozoic carbonate rocks previously deformed by Miocene regional contraction and seem to rejuvenate the intermittent basins and control their further Plio-Quaternary evolution as continental intermountain basins [*Cavinato et al*., 2002; *Improta et al*., 2012]. In Abruzzo, the region of this study, the landscape is generally characterized by NW-SE mountain ranges and karstic plateaus, alternating with glacio-fluvial valleys and fluvio-lacustrine basins. Differently from other areas of continental extension around the world, the low-topography terrains have continental infills that rarely exceed 100 or 200 m of thickness [*GE.MI.NA*, 1963]. The steep slopes of the mountain ranges are often being reshaped by widespread gravitational processes, such as rock avalanches or deep-seated gravitational slope deformations (DSGSDs) [e.g., *Nicoletti et al*., 1993; *Cinti et al*., 2001; *Scarascia Mugnozza et al*., 2006; *Di Luzio et al*., 2003; *Moro et al*., 2009; *Della Seta et al*., 2016].

The active extension is associated with moderate-to-large damaging earthquakes that have epicenters located within or near the Quaternary sedimentary basins. The identification of coseismic surface faulting has not been always straightforward as well as the direct association of the deep seismogenic sources with associated tectonic depocenters. In the case of the 1915 earthquake, contemporary accounts [*Oddone*, 1915] report coseismic surface faulting that seems to have clearly affected the intrabasin Quaternary sedimentary units and broke the ground surface. In the epicentral area *Oddone* [1915] and *Alfani* [1915] described a large landslide affecting the talus deposits positioned on a mountain front intersected by normal faults. Later on *Serva et al*. [1986] assumed the offset at the top of the slope deposits to be the primary coseismic slip of the 1915 earthquake causative fault, and several other researchers [e.g., *Benedetti et al*., 2013] consider this fault as active. Similarly, for the 1997–1998 Umbria-Marche seismic sequence, *Cello et al*. [1998] assumed the observed fault surface rejuvenations as being due to earthquake fault slip, while *Basili et al*. [1998] showed evidence that they were related to the gravitational sliding of the slope deposits. Nonetheless, several

subsequent studies attributed the entire fault exposure to earthquake slip and used their analyses for estimating fault slip rates and earthquake recurrence. In the case of the 2009 earthquake, the observed ground-surface fractures located within the sedimentary basin were interpreted as coseismic faulting [*Cinti et al*., 2011; *Lavecchia et al*., 2012], while seismological and geodetic data showed that the coseismic slip and aftershock distribution in the areas in question did not propagate to the surface, remaining at 2–3 km depth [*Cirella et al*., 2012; *Valoroso et al*., 2013].

Throughout the central Apennines straight to partially curved bedrock faults are exposed at various elevations along mountain slopes as bedrock scarps with heights generally of a few meters and in some cases between 10 and 20 m. These scarps are obvious geomorphic features partially covered by Quaternary continental deposits. Most frequently, these deposits drape the hillslopes with gently sloping aprons and fans of colluvial gravel and/or breccia and soil and are generally present both above and below the fault surfaces. Towards the upper edge of the scarps, the fault surface become less evident and in most cases is severely fractured and affected by karstic weathering [*Giaccio et al*., 2002]. These bedrock fault surfaces have been interpreted as the free faces of active and seismogenic normal faults, initially by *Bosi* [1975], who has classified them in four classes of activity based on their geomorphic characteristics and their structural relationships with continental Quaternary deposits. In the following decades, even though Bosi himself, and coauthors [*Bosi et al*., 1993], acknowledged that the fault surface exposure in the central Apennines mountain slopes can also be due to nontectonic processes, the hypothesis of the tectonic origin has been adopted by several scholars [e.g., *Roberts and Michetti*, 2004; *Benedetti et al*., 2013] without addressing and studying the factors that control the process.

Various techniques have been used to obtain slip rate estimates in the central Apennines. Topographic analysis and measures of long-term displacement of bedrock layers across bedrock fault surfaces yielded vertical slip rates in the range of 0.33–2.0 mm/yr [*Bubeck et al*., 2015; *Morewood and Roberts*, 2000; *Piccardi et al*., 1999; *Roberts and Michetti*, 2004]. Cosmogenic nuclide studies, attributing earthquake slip to the changes in ^{36}Cl concentration along dip of the fault surface, resulted in slip rates of 0.2–1.3 mm/yr [*Benedetti et al*., 2013; *Schlagenhauf et al*., 2010; *Tesson et al*., 2016]. Values that fall within these intervals were obtained also from paleoseismological trenches dug in the fault hanging wall at sites close to the contact with the bedrock fault surface [*Galli et al*., 2012]. Although these techniques are very different from one another, all of them have the following two assumptions in common: (1) postglacial slope stability and (2) fault surface exposure solely attributed to earthquake slip. That the sites chosen to study fault displacement have to be more carefully selected was acknowledged recently by *Bubeck et al*. [2015], who recommend avoiding erosional features like active outwash gullies (see *Piccardi et al*. [1999] for comparison). More recently, *Tesson et al*. [2016] seem to have included this recommendation, although they still make the same two assumptions described above. It is also worth noting that aseismic tectonic slip was not recognized as a possible contribution to the bedrock fault exposure. Available pertinent literature for the study area recognizes aseismic slip for structures not recognized as active faults [e.g., *Amoruso et al*., 2002]. Although it is well known that mountain terrains reveal valuable tectonic information, that information is interwoven with effects of surface processes such as regolith production and weathering, soil formation, sediment compaction, sediment downslope and fluvial transport, and landsliding [*Selby*, 1993; *Densmore et al*., 1998]. When addressing the potentially active and seismogenic faults in mountainous terrains, the convolution of all these processes cannot be neglected. Noting that this was the case in most studies on bedrock normal faults in the central Apennines, we set up an experiment to gain insights on these processes, at least in regards to the combined effect of determining the fault surface exposure.

To our knowledge, no pertinent direct measures aimed at quantifying the processes related to fault surface exposure, and possibly the distinction among its possible various components, is available in the literature. The scope of our study is thus to investigate the nature of bedrock fault surface exposure process and to quantify it by means of direct observations. We here investigate if the tectonic slip is really the only contributing factor in exposing the fault surfaces and verify if reliable estimates of the fault slip rates can be obtained for subsequent use in seismic hazard studies. To this end, we repeatedly measured the relative position between reference markers on the bedrock fault surface and the contact with eluvium/colluvium material that is found directly at its bottom. We surveyed 23 locations on 12 normal faults in the central Apennines for 3.4 years (Figures 1 and 2). During the observation period, the eluvial/colluvial material was cumulatively

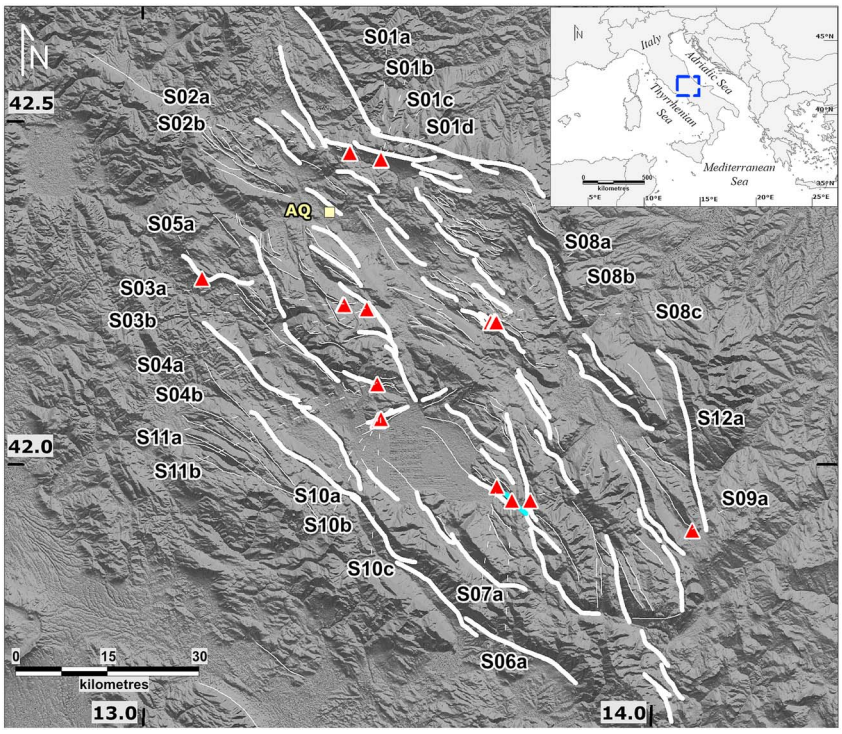

Figure 1. Extensional fault systems of the central Apennines from *Schlagenhauf* [2009]. The bedrock fault surfaces surveyed in this work are highlighted by using the classification adopted by *Schlagenhauf* [2009]: the thick white lines indicate the primary active faults, and the thin white lines indicate the secondary active faults. The triangles show the measurement sites (Table 1 and Figure S1). Notice that S06a is located on an exposed fault surface (turquoise line), which was not mapped as an active fault in previous studies. AQ: city of L'Aquila.

offset on the order of several centimeters relative to the reference markers on the bedrock fault surfaces. In all cases except one, the apparent offset contributed to progressively exposing the fault surfaces and to heightening the fault surface. All the measured fault surface exposures took place without intervening earthquake slip and varied significantly both temporally—between consecutive measurements—and spatially—even at short distance—along the same fault surface. Our results put serious doubts on the coseismic origin of bedrock fault exposure in the Apennines and its relevance for estimating tectonic slip rates and earthquake recurrence. Our results neither question the cosmogenic nuclide-dating method nor the age estimates of the fault surfaces so obtained. The method in question uses surface rock samples for measuring the concentration of cosmogenic nuclides. As such, it is an indirect observation of the process that exposes the studied rock surface without providing any insight on what the exposing process actually is. This is why studies using this technique on bedrock fault surfaces must resort to postulating the two points above. The same applies for methods using the height of the exposed fault surface for estimating the fault surface rejuvenation. We do however challenge the basic concept, so far adopted, that all the fault surface exposure detected by all of these methods is solely and purely of tectonic/seismogenic origin and caution against the possible use of slip rates so derived in seismic hazard studies.

2. Method

In order to identify the most appropriate study sites to monitor the relative position of fault surface contacts with Quaternary eluvial/colluvial deposits, we georeferenced regional geological and active fault maps overlain with regional/local digital relief models and satellite/aerial imagery. We used these data sets to analyze the local geomorphic and structural conditions along the mapped bedrock fault surfaces. We then carried out an extensive field reconnaissance and located several sites along the various fault surfaces (Figures 1 and S1 in the supporting information). In setting up the final network of measurement sites (MSs; Figure 1 and Table 1), we also considered the site accessibility conditions and the geomorphic characteristics of the

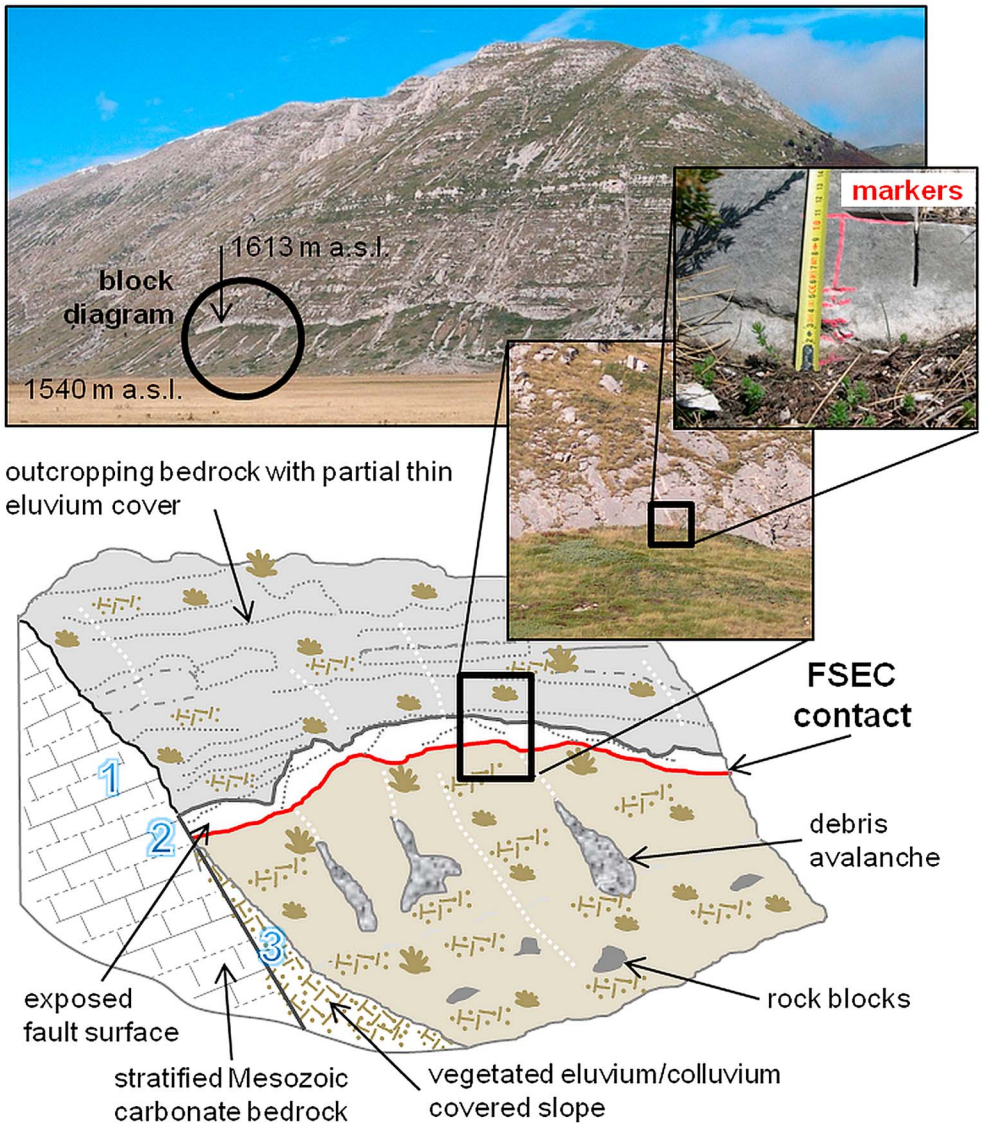

Figure 2. Panoramic view of typical bedrock fault surface and block diagram showing its geological conditions and processes. The insets show the close-up views of a measurement point, namely, the S04a (Figures 1 and S1 and Table 1). The probable dominant processes acting on the different sectors of the mountain slope are (1) convex slope with soil creep and chemical and physical weathering of the outcropping bedrock; (2) bedrock fault surface with rock block fall and slide and chemical and physical weathering; and (3) talus slope with downward movement of material by flow, slide, slump, or creep [from *Selby*, 1993].

exposed bedrock fault surface, choosing sites where the planar or curved fault surfaces are well exposed and show a low degree of fault surface degradation. We also selected the sites where the natural environment is better preserved and are well distant (at least in the slope direction) from anthropogenic activities (including buildings, roadcuts, and farming) (Figure S2). The only exception is the S07a (Figure 1) that is very close to a gravel road and for which we cannot estimate the possible effects that the passage of vehicles might have on the slope deposit instability.

Depending on the local conditions, each of the 12 monitored bedrock faults is represented by 1 to 4 distinct MSs in different positions along the fault surface, for a total of 23 MSs. At each MS we marked the position of the eluvial/colluvial deposit upper tip with a waterproof and well-recognizable painted line on the bedrock fault surface (Figure 2). At the time of each individual successive survey we measured the distance between the markers and the position of the eluvial/colluvial deposits. We refer to such distance as the fault surface-eluvial/colluvial (FSEC) offset. At the time of each measurement we cleared the measurement position of any

Journal of Geophysical Research: Earth Surface

10.1002/2016JF003953

Table 1. Data for the 23 MSs During the Monitoring Period[a]

Site ID	Fault Name	Fault Classification[b]	Longitude/ Latitude[c]	Elevation (m asl)	Strike[d]/Dip (deg)	Observation Period Δt (Years)	Cumulative Offset ±Uncertainty at k=2 (mm)	ER ±Uncertainty at k=2 (mm/yr)	R^2	F_{obs}/F_{crit}	ER Extrapolated Over 10^4 Years (mm/yr)[e]	CD-SR (mm/yr)	PA-SR (mm/yr)
S01a	Assergi east	Po/Pr	13.468/ 42.446	1330	90/40	3.321	16.8±4.8	6.8±1.3	0.74	4.3	1.5		0.2±<0.2[j]
S01b	Assergi east	Po/Pr	13.468/ 42.446	1330	90/40	3.321	12.0±2.8	5.8±0.8	0.65	2.8	1.3		0.2±<0.2[j]
S01c	Assergi east	Po/Pr	13.468/ 42.445	1329	90/40	1.151*	23.0±1.7	21.0±1.9	0.95	6.6	3.9		0.2±<0.2[j]
S01d	Assergi east	Po/Pr	13.468/ 42.446	1330	90/40	3.321	51.8±1.7	15.4±0.5	0.79	5.8	3.5		**0.2±<0.2**[j]
S02a[f,g,h,i]	Assergi west	VP/Pr	13.407/ 42.456	1597	126/67	2.844	−34.5±2.9	−10.2±1.1	0.56	0.4	N/A		**0.2±<0.2**[j]
S02b[f,g,h,i]	Assergi west	VP/Pr	13.407/ 42.455	1596	126/67	2.093	6±2.6	3.6±0.4	0.40	<0.1	0.8		
S03a	Campo Felice west	Po/S	13.394/ 42.234	1622	110/52	2.578	38.8±1.4	13.9±0.6	0.91	7.3	3		
S03b	Campo Felice west	Po/S	13.396/ 42.233	1621	113/51	2.578	26.8±1.4	9.4±0.6	0.90	6.7	2		
S04a	Campo Felice east	VP/Pr	13.444/ 42.228	1613	110/54	2.578	53.5±1.7	19.8±0.6	0.87	115.5	4.3	**1**[k]	**0.17**[l]
S04b[i]	Campo Felice east	VP/Pr	13.440/ 42.227	1611	112/55	2.578	20.8±1.7	5.0±0.6	0.34	0.4	1.1	1[k]	**0.17**[l]
S05a[g]	Fiamignano	VP/Pr	13.116/ 42.272	1137	120/40	2.499	73.5±1.9	25.6±0.9	0.77	3.3	5.5	N/A	0.83±<0.2[j] 1.27±0.4[m]
S06a	Serrone anthite-tic	N.M.	13.726/ 41.947	1339	320/56	2.323	21.8±1.4	8.9±0.7	0.86	20.5	1.9		
S07a	Fucino high	N.M./S	13.696/ 41.968	939	135/48	2.575	58.8±1.9	21.2±0.6	0.93	13.5	4.6		
S08a	Aterno valley	P/Pr	13.684/ 42.208	951	150/70	3.205	25.8±3.4	7.6±1.1	0.88	5.9	1.7		0.3±<0.2[j]
S08b[f,g,h]	Aterno valley	P/Pr	13.695/ 42.200	834	126/66	1.953*	10.7±1.2	4.5±0.6	0.43	0.4	0.9		0.3±<0.2[j]
S08c[f]	Aterno valley	P/Pr	13.695/ 42.200	834	126/68	3.205	54.0±1.7	15.0±0.4	0.85	7.3	3.4		0.3±<0.2[j]
S09a[i]	Pizzalto	P/S	14.081/ 41.904	1397	105/54	2.189	3.2±1.3	2.9±0.8	0.62	<0.1	0.6	**1.4**[n]	
S10a[g]	Tre Monti	VP/Pr	13.463/ 42.065	997	70/72	2.575	40.0±17	17.0±0.6	0.96	32.2	3.7	**0.2**[k]	**0.16**[l] **0.43±<0.1**[m]
S10b[g]	Tre Monti	VP/Pr	13.463/ 42.065	997	70/72	2.575	22.8±1.4	8.7±0.6	0.90	8.8	1.9	**0.2**[k]	**0.16**[l] **0.43±<0.1**[m]
S10c[g,h,i]	Tre Monti	VP/Pr	13.468/ 42.067	1010	40/66	2.575	17.0±1.3	5.7±0.6	0.41	0.7	1.2	0.2[k]	**0.16**[l] **0.43±<0.1**[m]
S11a[f]	Magnola	VP/Pr	13.461/ 42.118	1345	90/42	3.167	46.0±1.7	13.2±0.5	0.60	1.8	3	**1.3**[k]	**0.23**[l] **1.0±<0.1**[m]

Table 1. (continued)

Site ID	Fault Name	Fault Classification[b]	Longitude/ Latitude[c]	Elevation (m asl)	Strike[d]/Dip (deg)	Observation Period Δt (Years)	Cumulative Offset ±Uncertainty at $k=2$ (mm)	ER ±Uncertainty at $k=2$ (mm/yr)	R^2	F_{obs}/F_{crit}	ER Extrapolated Over 10^4 Years (mm/yr)[e]	CD-SR (mm/yr)	PA-SR (mm/yr)
S11b[f]	Magnola	VP/Pr	13.461/ 42.118	1345	90/42	3.167	50.0±1.6	13.9±0.5	0.63	1.8	3.1	**1.3**[k]	**0.23**[l] **1.0±<0.1**[m]
S12a	Valle del Giovenco	P/Pr	13.762/ 41.947	1211	180/65	2.326	10.4±1.3	4.5±0.6	0.70	1.7	1	**0.5**[k]	**0.27±<0.2**[j]

[a]The shortest observation period for an individual MS is 2.21 years. The exceptions are the two MSs marked with an asterisk next to their observation time; S01c was established as a new MS after it was freshly exposed below the S01a-b MSs (October 2014), while S08b was interrupted after the July 2014 measurement (Δt=1.95 years) because it was disturbed by an unknown cause. The offset and ER uncertainty is an extended uncertainty at the 95% level of confidence (coverage factor; k=2). R^2 is the regression coefficient of determination for the ER linear model. F_{obs}/F_{crit}: F test parameters; if $F_{obs} \geq F_{crit}$ the linear ER model fits the data, and if $F_{obs} < F_{crit}$ the linear ER model is rejected. CD-SR: slip rates obtained through dating exposed surfaces with ^{36}Cl. NA is where the method of cosmogenic nuclide dating [*Benedetti et al*., 2013] was not applicable to resolve for slip rate. PA-SR: slip rates obtained through considering the height of the fault surface and the presumed estimate of its age. In bold, fault slip rates calculated at the same sites as our exposure rates.

[b]Classification of fault activity likelihood from *Bosi* [1975]: VP=very probable and P=probable/Po=possible and hierarchy classification from *Schlagenhauf* [2009]: Pr=principal and S=secondary; N.M.=not mapped as an active fault in any of the considered previous studies.

[c]Coordinates datum is WGS84.

[d]Local fault strike (may differ from overall fault strike as mapped in Figure 1) and dip are also indicated. See Figure 1 for MS locations.

[e]We applied the time observation period correction for our ERs in order to extrapolate them to geological times comparable to the periods (10^4 years) for which the SRs found in the literature were calculated. The S02a MS is governed by accumulation and not erosion, thus the applied time extrapolation valid for erosion does not apply; marked as N/A.

[f]Measurement sites within 100 m distance from an outwash gully.

[g]Measurement sites classified as belonging to fault surfaces of pure tectonic origin by *Bubeck et al*. [2015].

[h]Measurement site artificially disrupted between 23 July and 13 December 2014.

[i]Measurement sites for which the ER linear model is rejected.

[j]*Benedetti et al*. [2013].

[k]*Tesson et al*. [2016].

[l]*Morewood and Roberts* [2000].

[m]*Roberts and Michetti* [2004].

[n]*Bubeck et al*. [2015].

Journal of Geophysical Research: Earth Surface

10.1002/2016JF003953

possible accumulated loose organic material (e.g., leaves) and larger rock debris in order to always measure the relative position of the markers with respect to the eluvial/colluvial deposit. Whenever the FSEC offset has lowered between two consecutive surveys, we marked the new position of the FSEC contact, thus increasing the number of markers. The measurements were taken in the direction of the fault surface maximum slope and executed by more than one operator, in order to minimize possible biases, using a measuring tape and a laser range finder. Thanks to the simplicity of the measurement method, the sites require only a short presence during each survey, thereby causing a minimal disturbance to the sites themselves. The slope deposits do not seem to be disturbed during the access to the sites as we have not detected any lowering of the eluvium/colluvium due to this cause. During the observation period we have not registered any extreme weather events like exceptional rain/snow storms or flooding that might have contributed to sudden mass-wasting episodes along the surveyed mountain fronts. The only well-known such event is an earth-and-debris flow occurred in May 2009 not very far from, but that did not affecting, S01a-d, i.e., before the start of our surveys.

We registered both incremental and total offsets as the average value of individual measurements for all the markers for each MS and selected the reference marker as the offset representative for each MS. In most cases (17 MSs) the reference marker coincides with the position of the FSEC contact at the time of the first measurement. In specific cases (six MSs), when that contact got covered between the first and the second measurements, the reference marker is the first lowest positioned marker above the FSEC contact at the time of the second measurement at that MSs. In order to keep track of the conditions at the time of each measurement we took photos for each MS and used them to compare the situation at the time of each following measurement. The simplicity of the method implies that all measurement uncertainties are from easily controllable sources, such as the resolution of the measurement tape, the possible tilt in either directions from the maximum slope (not exceeding 10°), and the 2 mm width of the marker painted line (Figures 2 and S4). We consider the offset uncertainty with a normal distribution and report it as its expanded value at the 95% confidence level (coverage factor $k=2$).

We investigate the temporal FSEC offset trend to derive an average exposure rate (ER) of the observed fault surfaces occurred during the 3.4 years of our experiment and use this value as a term of comparison with the presumed tectonic slip rate equated to the long-term fault surface exposure rate by previous studies for the same faults and also the same MSs. Knowing that each measurement is independent from the others and assuming that the measured offsets are normally distributed, we derive the average ER for each site through a linear regression model based on ordinary least squares and test the regression through the analysis of variance (F test) at the 95% significance level. The uncertainty of the regression model ($k=2$) is also considered.

3. Results

Our general geomorphic and geological investigations show that the studied faults are planar to curved carbonate surfaces showing different degrees of karstification and fracturing. On the slopes above the exposed fault surfaces unfaulted bedded carbonates or carbonate blocks outcrop in few of the studied sites, while for all of the sites the updip prolongation of the fault surface is difficult to follow and map due to soil and vegetation cover. At the lower edge, the fault surface is in contact with soil, eluvium/colluvium, vegetation, or a combination of the three. Along strike the bedrock fault surface is not exposed as a continuous planar or curved fault surface for prolonged distances. Instead, it is frequently interrupted by zones exhibiting intense fracturing or disengaged blocks. It is also frequently observed that the fault surface is discontinuous along strike and cannot be followed in the topographic profile due to either breccia or soil and vegetation cover (i.e., the scarp does not affect the cover material). At the scale of individual patches of exposed bedrock fault surfaces, a semicircular rim of the overlying material is typically observed. The apex of the rim is generally positioned at the center of the exposed fault and tapers off toward both extremities (Figure S2).

The systematic use of previously compiled regional active fault maps allowed us to intentionally include in our surveys a wide range of structural and geological conditions. We are thus able to compare the observations at our MSs with the four classes of activity of "very probable," "probable," "possible," and "dubious" (terms translated from the Italian) attributed to the studied faults by *Bosi* [1975], as well as the fault hierarchical classification of "principal" or "secondary" used by *Schlagenhauf* [2009]. We also identified and inspected the locations that were sampled for cosmogenic nuclide dating by *Benedetti et al.* [2013], and

Schlagenhauf et al. [2011]. By doing so, we have a direct comparison between the published results of fault surface exposures and our results. In particular, we also considered the discrimination made by *Bubeck et al*. [2015] on the geological stability of some mountain slopes, and thus included in our study those sites considered of pure tectonic origin as well as the sites regarded as having been affected by different morphogenic factors other than tectonics, like active gully outwash erosion.

Our final data set consists of 23 MSs along 12 different faults (Figure 1). Nineteen of these MSs are located on NW-SE faults on SW facing slopes, three are located on a WSW-NNE fault on a SSE facing slope (S10a-b-c), and one is on a SE-NW fault on a NE facing slope (S06a). Based on the classification by *Bosi* [1975], 10 of the MSs are located on faults with very probable evidence of recent activity: 5 of them on faults for which the activity is probable, 6 on faults with possible evidence of activity, and none on faults with dubious evidence of activity. Following the distinction between principal and secondary active faults by *Schlagenhauf* [2009], 18 of our MSs are located on principal faults and 4 of them on secondary faults. S06a is located on a fault that was not previously mapped as an active one; thus, it has no preassigned classification, while the S07a lies on a fault not recognized in the fault compilation by *Bosi* [1975]. The S06a hosting fault is much shorter than all others and dips toward the opposite direction with respect to the majority of the other faults. Nonetheless, it exhibits the same geomorphic characteristics of all other faults and was included in our data set as a term of comparison. All of the analyzed fault surfaces exhibit various degrees of weathering and karstification and are partially covered by Quaternary deposits and eluvium/colluvium material.

We repeated FSEC position measurements during the period from August 2012 to December 2015. Although the surveys started at different times for different sites, each MS has been monitored for at least 26 months (2.1 years) and visited for a minimum of 4 times (Figure S3). The only exceptions are S01c that was established after having been freshly exposed below S01a-b and S08b that was artificially disturbed and thus abandoned. The results of all measurements and analyses are shown in Table 1 and Figure 3a. The entire data set for all MSs is presented in Figure S3.

The FSEC cumulative offset in the survey period is on the order of a few millimeters to a few centimeters with uncertainties in the range of tenths to a maximum of a few millimeters. Except for S02a, all cumulative offsets correspond to downward movement (i.e., increased exposure). However, we observed that between individual measurements the offset occasionally reversed its polarity or remained unchanged, resulting in unstable offset trends. Only for S01c, S08b, S04a, and S10a (Figures 3 and S3) the average measured offsets increased continuously. The first two MSs were surveyed only 4 times because one was only recently exposed (S01c; October 2014), and in the other case the FSEC contact was artificially disrupted (S08b); therefore, these simpler trends might be due to the shortness of the observation period. The other two MSs have been monitored for a longer period (eight surveys) and show a slow, though constantly increased or unchanged average offsets. The most variable offset is that of S09a that exhibits an oscillatory pattern.

The offset is variable in amount and polarity also for MSs located a short distance from one another along the same fault surface, such as the cases of S01a-b-c-d (Figure S2). About a meter below the previously marked FSEC contact at S01a-b an irregular patch (0.5 m^2) of fresh fault surface was first observed to be exposed (S01c) in October 2014. This event seems to have overtaken the overall exposure process, evidenced by a notable decrease of exposure for S01a-b. For S11a-b, in December 2014, we found that a loose soil wedge had collapsed sideways on the FSEC contact and partially covered the previously exposed part, thereby altering the increasing offset trend with an abrupt change of polarity. Moreover, during the December 2015 survey, we found that both S11a and S11b were affected by a passage of boars coupled with debris avalanche initiated above both MSs. We consider this type of episode to be part of the process as they testify to the complexity and spatial variability of the fault surface exposure.

Besides the point measurements, the fault surface exposure is evidenced also by undulated lighter-color bands (Figures 2 and S2; likely due to humic acid leaching). Such white bands can be followed along the FSEC contact and testify to the lateral extent and variability of the exposure process.

The linear regression models for the 23 MSs (Table 1 and Figure 3) result in (1) positive ER in the two-digit mm/yr range for 10 MSs, (2) positive ER in the one-digit mm/yr range for 18 MSs, and (3) a negative ER in the two-digit mm/yr range for one MS. More specifically, the FSEC contact at S02a has been moving upward

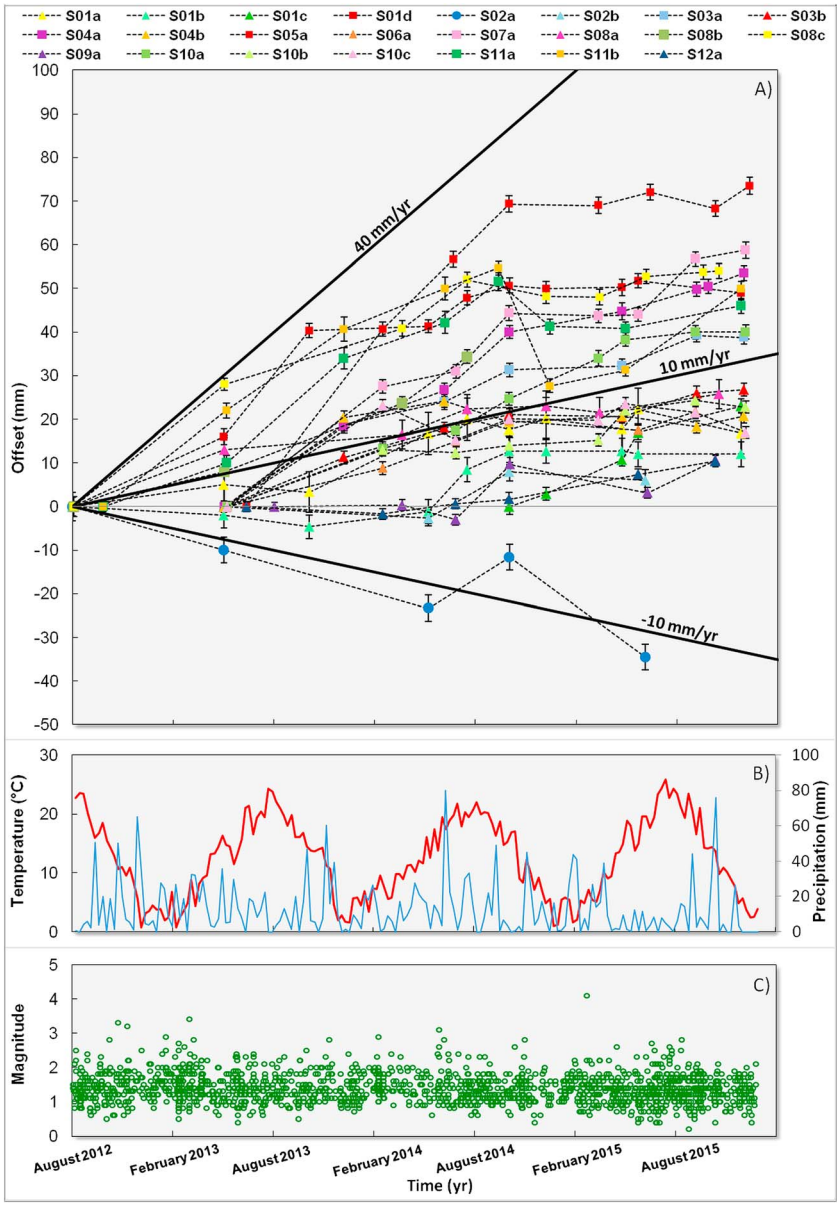

Figure 3. (a) Fault surface exposure trend for the 23 measurement sites. Notice that for only one site the cumulative trend is negative. The straight solid lines of −10, 10, and 40 mm/yr trends are shown for comparison. The vertical bars represent each offset measurement combined uncertainty at $k=2$ (95% probability level). (b) Weekly averaged temperature and rainfall (from CETEMPS; http://cetemps.aquila.infn.it/index.php?option=com_wrapper&view=wrapper&Itemid=127), respectively. (c) Seismicity sampled within a buffer of 20 km from around the measurement sites and depth shallower than 15 km (from ISIDE; http://iside.rm.ingv.it/iside/standard/index.jsp).

during most of the observation period apart from an episode in which it moved downward. The *F* tests confirm that the linear offset model is a statistically acceptable trend for 18 MSs, whereas it is rejected for S02a, S02b, S04a, S09a, and S10c (Table 1).

We do not observe a correlation between the ERs and the two fault classifications reported in Table 1. Considering that of *Bosi* [1975], the faults with a very probable evidence of recent activity have ERs of either one-digit or two-digit mm/yr values; the same is found for faults classified with a probable and possible evidence of recent activity. S02a lies on a fault classified with very probable evidence of recent activity and is in fact the only MS with a negative ER trend (i.e., the fault surface is being covered by accreting eluvium/colluvium). The four faults classified as secondary by *Schlagenhauf* [2009] span in the one-digit to

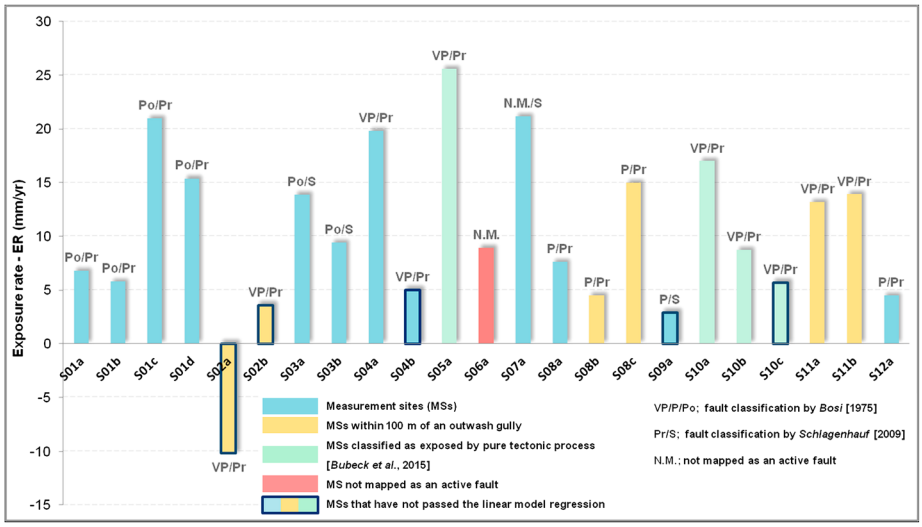

Figure 4. Characteristics of the exposure rates (ERs). The label for fault classification is written in the following form: classification by *Bosi* [1975]/classification by *Schlagenhauf* [2009]. For further reference, see Figure 1 and Table 1.

two-digit mm/yr ERs and are thus statistically not different from the faults classified as principal. Even S06a—which was intentionally positioned on a fault that was not classified as active—has an ER in the same range as the rest of the MSs (Figure 4).

The comparison of ERs for the MSs that lie within a 100 m distance from an outwash gully (Table 1 and Figure 4) with respect to the MSs located farther away from such features does not show any significant difference from one another. Counterintuitively, S02a that is the only MS with a negative ER trend lies within 100 m from the center of an active outwash gully. We also compared the ER for MSs (S05a and S10a-c) lying on fault surfaces classified as having been exposed through a pure tectonic process by *Bubeck et al.* [2015] with respect to MSs lying on faults that, based on the same study, were classified as being influenced also by other processes (S11a-b). Such a comparison shows that both types of MSs have ERs in the two-digit mm/yr range. Also, those MSs positioned on fault surface exposures classified as being due to a pure tectonic origin have ERs in the one-digit mm/yr. S05a, the MS with the highest ER lies on a part of a fault classified as having pure tectonic origin, although it is adjacent to the patch of the fault surface for which also a gully outwash process was recognized.

Cases where MSs lying along the same fault surface having comparable ERs are present (S01a,b and S11a,b), although the ones for which ERs vary substantially are prevailing (e.g., S03a,b; S04a,b; and S08a,b,c). In the case of the Assergi East fault surface, S01c, positioned on a fault patch that was freshly exposed right below S01a and S01b, has an ER 3 times faster than the above lying MS, although its observation period is shorter. It is also observed, as pointed out above, that the measured offsets for S01a-b have decreased substantially, or have stopped entirely, since the new fault surface at S01c started to be exposed. A great deal of variation in the ER is observed also along the Tre Monti fault surface, especially for S11a and S11b that are very close to each other. Thus, we observe that both temporal and spatial ER variations, also at short distance between MSs, occur along the same fault surface.

Our ERs cover a period of a few years, while the presumed slip rates derived from various dating methods cover a period of a few thousands to a few tens of thousands of years. *Gardner et al.* [1987] have shown that both tectonic and erosional processes are not independent from the time observation interval and that they should not be directly compared over different time scales. Applying the empirical relation that accounts for the systematic decrease in average rates of surficial erosional processes with increasing time interval (equations (2) and (6) from *Gardner et al.* [1987] and Figure S5) results in ERs being very similar to the slip rates obtained from the application of the cosmogenic nuclide concentration method [*Benedetti et al.*, 2013] (e.g., Velino fault with respect to S11a-b). Similar results are obtained by comparing our ERs with slip rates derived from the method of correlating the scarp height with the age of displaced stratigraphic units [see *Morewood*

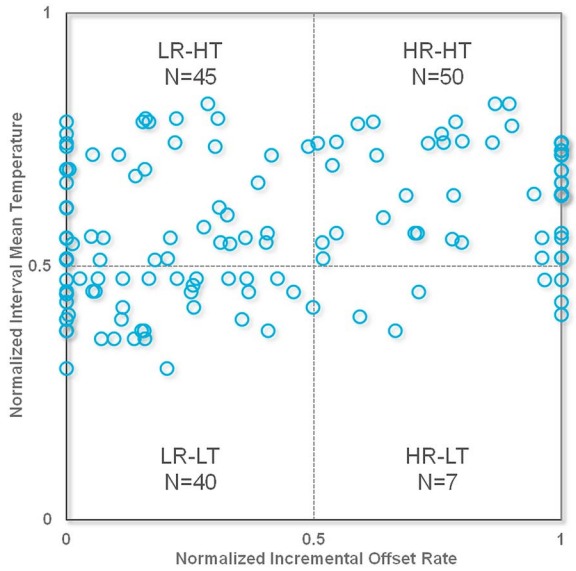

Figure 5. Diagram exploring the relationships between incremental offset rates R [$R=(D_n-D_{n-1})/(t_n-t_{n-1})$, where D is the offset and t is the time of every nth measurement] and average temperature (T) during the time interval t_n-t_{n-1}. Both axis are normalized using feature scaling: $x'=[x-\min(x)]/[\max(x)-\min(x)]$, where x is the original value and x' is the normalized value. Labels of the four quadrants are LR=low offset rate, HR=high offset rate, LT=low temperature, and HT=high temperature; N=number of data points. The values of S11a-b altered by the passage of wild boars were removed from these counts. We observe that higher offset rates have occurred more frequently during the warmer periods. The numeric values for each normalized offset rate and temperature are shown in Figure S3. The offset trend for each of the measurement sites with respect to the temperature is shown in Figure S6.

and Roberts, 2000; *Roberts and Michetti*, 2004] (e.g., L'Aquila fault with respect to AS03a-b; Campo Felice fault with respect to S04a-b). Therefore, when the ERs and slip rates are compared without considering the observation time correction, there is a 1 to 2 orders of magnitude difference between the two estimates. Conversely, when the observation time interval effect is considered (10^0–10^1 with respect to 10^3–10^4 years), the maximum differences collapse down to 1 order of magnitude and generally the estimates become comparable, if not almost the same (Table 1). This implies that expanding our ERs from modern time to geological timescales reinforces the conclusion that the fault surface exposure can be entirely due to causes different from surface faulting.

4. Discussion and Conclusions

We provide, for the first time, quantitative evidence of nontectonic FSEC contact displacement along supposedly active bedrock faults in the central Apennines (Italy), based on direct FSEC offset measurements repeated over a 3.4 year long period. Before starting the experiment, to our knowledge, no quantitative studies on possible nontectonic movements of the FSEC contact were documented. Conversely, the post Last Glacial Maximum (LGM) FSEC stability was postulated in many previous works and used as a reference for rating tectonic faulting [*Roberts and Michetti*, 2004]. We put particular care in marking the FSEC contact positions and in estimating measurement uncertainties that for the characteristics of the method are small and controllable. The resulting cumulative offsets are 1 order of magnitude larger than the incurred errors and uncertainties, thereby confirming the representativeness of the detected movements. Despite the high variability of incremental offsets (Figures 3 and S3), a consistently increasing trend of the fault surface exposure characterizes the majority of sites (Figure 3a).

As regards our observation period, we verified the possible dependence of the FSEC contact behavior from, or in connection with, a few contemporary potentially causative morphogenic or tectonic factors. For example, by comparing the registered precipitation (rain/snow) with our measured offset data, we observe that downward FSEC contact movements increased both during the periods of strong and weak precipitation (Figure 3b) with no particular pattern. Except for few soil collapse events that tend to cover the previously exposed part of the fault surface and occurred in different periods, we observe a tendency of more intense

downward FSEC contact movements to occur more frequently in the warm season, while less intense movements occur in similar proportions during the entire year (Figures 3b, 5, and S6). This observation might be partially explained by the winter snow cover that buffers the subsurface deposits from diurnal temperature changes and temporarily decreases erosion rates [*Pelletier and Rasmussen*, 2009].

During the monitoring period no major earthquake occurred within the surveyed region (maximum M_l=4.1; Figure 3c), thereby confirming the observed fault exposure process not having a seismic origin—neither as on-fault earthquake slip nor as ground motion secondary effects (e.g., soil compaction and slope failure).

The location of bedrock fault surfaces, and more the location of selected measurement points, coincides with at least one type of active landslide process documented in the inventory of active landslides [*Trigila et al*., 2015; *Trigila et al*., 2010] for 13 out of 23 measurement points (Figure S7). That is to say that independent systematic studies show active movements of nontectonic origin impacting the studied sites and faults. The quantity of different types of landsliding movement has not been established in the national inventory, but local studies corresponding to the zones of our S06a and S07a registered several to tenths of mm/yr oscillatory movements attributed to deep-seated gravitational slope deformation (DSGSD) [*Moro et al*., 2009]. Extensive bedrock avalanches related to the DSGSDs have been recognized throughout the central Apennines [*Di Luzio et al*., 2003; *Scarascia Mugnozza et al*., 2006; *Bianchi Fasani et al*., 2014; *Della Seta et al*., 2016]. In particular, *Bianchi Fasani et al*. [2014] point out that backlimb slide-wedge rock avalanches affect carbonate rocks of fault-bounded ridges with a combined sliding and rock-wedge failure mechanism. Several rock avalanches mapped in the central Apennines affect mountain slopes that are among those characterized by presumed active normal faults.

Rock slopes undergoing long-term effects of weathering and gravity may gradually deform or creep downslope, leading to geological structures such as bending, buckling, fracturing, or even progressive failure [*Chang et al*., 2014]. *Discenza et al*. [2011] interpreted the central Apennines gravitational slope deformation as rock mass creep evolving into rock mass spreading and modeled its horizontal displacement on the order of several tenths of millimeter per year. Given these considerations, we propose the observed fault surface exposure in the study region as being mostly attributable to gravitational landsliding and mass creep slope deformation aided by erosion and slope degradation.

Tectonic slip rates and earthquake recurrence for the central Apennines normal faults have been proposed by considering exposed bedrock fault surfaces and their slope-deposit partial cover in either of three ways: (1) by measuring the scarp height and dividing it by the presumed age of uncover [*Roberts and Michetti*, 2004]; (2) by identifying peaks in the fault surface exposure chronology obtained through cosmogenic isotope concentration and attributing these peaks to coseismic exposure [*Benedetti et al*., 2013]; and (3) by identifying evidence of brittle, supposedly sudden, displacement within the slope deposit covering the fault surface through paleoseismic trenches [*Galli et al*., 2012]. Collectively, these techniques resulted in 0.2–2.0 mm/yr slip rates and mean earthquake recurrence of surface faulting events in the 400–4200 year range. All these methods, however, require slope-deposit stability during the interseismic period and postulate that fault surface exposure increases only through coseismic faulting. We have shown here these assumptions not to be valid, and we thus contend that these methods are not suitable for revealing rates of tectonic activity unequivocally, even at sites where the geomorphic processes are not as evident as in those cases previously defined as of pure tectonic origin by *Bubeck et al*. [2015]. Also, the S06a, a site located on a fault surface not mapped as an active fault, has the ER in the same range as the rest of the sites, thus reinforcing the nontectonic origin of the measured exposure process.

Compared to slip rates obtained through the above described approaches, our ERs for the same fault surfaces are 1 to 2 orders of magnitude higher. The fastest ERs are registered at S05a; the MS (started at month 10 of the experiment) at which a scarp height of 10 m would be exposed in 400 years by assuming the linearity of the ER derived from the 2.5 years of observations. The same 10 m would take 2000 years to be exposed for one of the slowest exposing MS, the S04b. Compared to ages of 2200 and 9400 years for the top of Fiamignano (S05a) and Campo Felice (S04a) fault surfaces [*Benedetti et al*., 2013] that means 5.5 and 4.7 times faster exposure, respectively.

Our ERs, however, cannot be linearly extrapolated over geologic timescales. Erosion and deposition processes, when analyzed over different time scales, are affected by the so-called "Sadler effect," which

implies a power law decrease of their rate with increasing length of the observation period [e.g., *Sadler*, 1981; *Schumer et al*., 2011; *Finnegan et al*., 2014]. Such an effect originates from the intrinsic characteristics of these processes in which the intermittency of deposit accumulation and deposition hiatuses and the intermittency of erosion and denudation stasis at a point combines in various ways with the spatial distribution of their occurrences [*Schumer and Jerolmack*, 2009; *Ganti et al*., 2011]. As the time window of observation increases, so does the likelihood of registering periods with neither erosion nor deposition [*Finnegan et al*., 2014]. Considering this, the process responsible for the central Apennines bedrock fault surface exposure is interpreted as having a negative power law distribution (Figure S5) that, when corrected for the time interval bias of our short-term rates, collapse down to approach or to even match the long-term exposure rates attributed to fault slip on the same bedrock fault surfaces (Table 1).

The maximum total FSEC contact offset we registered is of 73.5 mm in 2.5 years at S05a. Supposing that the exposure process carries on for about 40 years at this rate, the total offset would be similar to the amount of a single-event surface displacement (SESD) of an M_w 7 earthquake (approximately 1.2 m). The slowest of our sites would produce the same offset only in 240–330 years. Therefore, the time required for weathering and erosion to expose the fault surface by an amount that resembles a coseismic SESD is much smaller than the uncertainty associated with the dating of cosmogenic isotope concentration peaks used by *Benedetti et al*. [2013], *Schlagenhauf* [2009], and *Tesson et al*. [2016] to detect an event of presumed earthquake slip. It is worth recalling that even though the cosmogenic nuclide dating is a well-benchmarked method, it is not a direct measurement of the exposure process. Its application to derive fault surface exposure rates is subjected to errors and uncertainties greater than typical ranges of both space and time of either erosional or tectonic processes. We remark that it is not the validity of the dating methods that is questioned here, but rather the interpretation of fault surface exposure attributed to tectonic processes alone.

The ERs for different MSs positioned along individual fault surfaces vary both spatially and temporally (Figure S3). These differences are within the same order of magnitude, typically varying by a factor of 2 to 4. In general, these differences are bigger when comparing MSs with different observation times, as it is the case for S08b and S08c, whose ERs vary by a factor of more than 3 (notice that S08b has been abandoned after it was artificially disrupted in the late 2014). Another example of how different observation times affect the ER is the fault surface measured at S01a, b, and c. The fastest ER is registered for S01c that has the shortest observation period among all MSs for having started to be exposed more than 24 months (2 years) after our survey began. In fact, the fast exposure of S01c seems to have taken up almost the entire exposures of S01a and S01b that are located just above on the same fault surface and whose offsets have drastically diminished with the new exposure of the fault surface patch below them. Compared to S01d that lays a few tenths of centimeters from the just described group of MSs, S01c has comparable values (21.0 ± 1.9 mm/yr for S01c with respect to 15.4 ± 0.5 mm/yr for S01d). Spatial variations along a single-fault surface are also reported for slip rates calculated by relating fault surface heights with the age of displaced deposits [*Morewood and Roberts*, 2000; *Roberts and Michetti*, 2004]. As is the case of ER, the slip rate differences are typically within the same order of magnitude and vary up to a factor of 4. For a few cases (e.g., L'Aquila fault [*Roberts and Michetti*, 2004] or Tre Monti fault [*Morewood and Roberts*, 2000]), slip rate differences span across an order of magnitude. The fault surface height differences may therefore not be due to different amounts of accumulated slip along strike but rather represent the natural variability of the exposure process through weathering and erosion of the loose or weakly cemented Quaternary slope deposits with respect to the harder Mesozoic carbonates of the bedrock fault.

Slope-deposit stability, along with diminished bedrock weathering and erosion, was postulated by considering that the warmer climate after the LGM had favored vegetation cover and reforestation. For this reason, several scholars assumed the tectonic origin as the only possible, or most plausible, explanation for the increased fault surface exposure, or the enhanced heights of bedrock fault surface, during the Holocene [*Galli et al*., 2012; *Roberts and Michetti*, 2004]. This assumption was made while somehow neglecting that minor climatic changes and lithology contrasts also play a role in landscape shaping. On the one hand, three climate events with changes in plant biomass toward aridification occurred in the central Mediterranean after the LGM (8200 years B.P., 6000 years B.P., and soon after 3000 years B.P.). In Italy they overlapped with human impact since the Bronze Age (approximately 4400 years B.P. [*Sadori et al*., 2011]) and were followed by an increased human-driven deforestation in the Medieval Period (approximately 600 Common Era) [*Mensing*

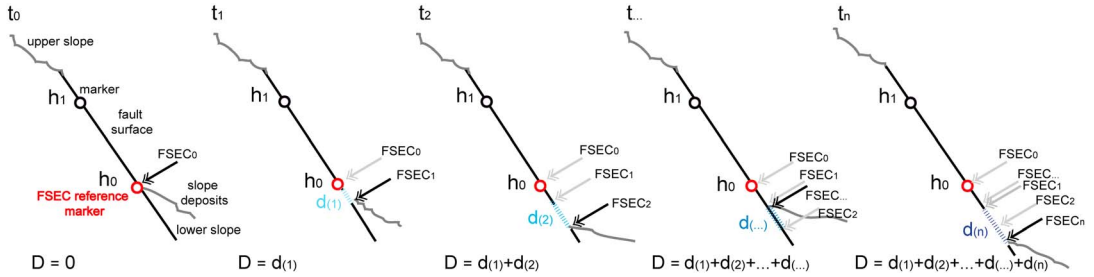

Figure 6. Interpretive sketch model of the fault surface-eluvium/colluvium contact evolution depicting incremental (*d*) and cumulative (*D*) offset over a given time period (t_0 to t_n). The dashed lines represent the free face formed between successive surveys. Note that we monitor the lower edge of the exposed fault surface, i.e., its contact with the hanging wall material.

et al., 2015]. The most probable ages of stronger earthquake activity deduced by *Benedetti et al*. [2013] from the concentration of cosmogenic nuclides show to be time clustered at 11 ± 1, 4.5 ± 1, and 1.5 ± 1 kyr ago for the majority of the sampled fault surfaces. These periods are subsequent to the LGM and seem to alternate with the aridification and human-driven deforestation events, processes that are likely to have influenced the rate at which the deposit cover was removed from the mountain slopes, enhancing the synchronous exposure of bedrock fault surfaces on a regional scale. On the other hand, the lithological contrast between the less erodible bedrock and the loose to weakly lithified slope deposits can have further favored slope profile degradation in correspondence of the latter, thereby increasing the scarp height and fault exposure.

We propose that the results of fault surface exposure, especially over shorter observation periods, depend on the near-site conditions of the sampled point. Known exogenic factors contribute or even govern the exposure process, resulting in periods of progressive exposure alternating with periods of quiescence or even recovering of the already exposed patches of the fault surface. Over longer observation periods though, the governing processes produce increased fault exposure (Figure 6). Our short time frame, over which the large majority of the MSs have increasing cumulative FSEC offsets, seems to be too short to have captured exposure hiatuses. As we propose in the mountain slope exposure model (Figure 6), stagnant or even negative offsets (situation at time t_n; Figure 6) contribute to slowing down the long-term exposure resulting in the negative power law distribution explained by the Sadler effect. Such characteristics prevent the exposed fault surface from reaching preposterous heights over longer time periods as it would be the case if considering our mean ERs as a steady state process. Indeed, the height of the bedrock fault scarps is generally less than 20 m.

In conclusion, the exposed fault surfaces analyzed in our study have long been considered as the expression of active and seismogenic normal faults based on geomorphic analysis and shallow probing. We demonstrate that their monitored exposure is of nontectonic origin, a result that contradicts the slip rates obtained by attributing all of the exposure to earthquake origin. Our results suggest that a new course of studies is necessary in order to verify whether the bedrock faults analyzed here are the actual tectonic players of Apennines active extension and seek reliable strategies to assess their activity. Further, we highlight the importance of considering deep-seated gravitational slope deformation, mass creep, erosion, and slope degradation processes in interpreting the geomorphic signature of tectonic structures in mountainous regions.

These findings have important consequences for seismic hazard studies that aim at exploiting active fault data. The need for reliable fault slip rates is increasingly playing an important role in both time-dependent and time-independent seismic hazard studies [*Akinci et al*., 2010; *Field et al*., 2013; *Hiemer et al*., 2014; *Kastelic et al*., 2016; *Petersen et al*., 2013; *Stirling et al*., 2012; *Woessner et al*., 2015], and thus, the existence of a seismogenic fault, its geometry, kinematics, and rate of activity are fundamental information. Hence, it is of primary importance that the data collected on presumed active faults actually sample and represent the tectonic and seismogenic deformation or at least that their nontectonic component is removed.

4.1. Postscriptum

On 24 August 2016, while this work was under review, an earthquake of M_w 6.0 occurred in the central Apennines, with a NW-SE trending, SW dipping, normal faulting mechanism. The epicentral area is located ~80 km to the north of the area studied here. Preliminary postearthquake data (geologic field surveys and

interferometric synthetic aperture radar) show an important downward mobilization of slope deposits in correspondence of a bedrock normal fault in the northern part of the epicentral area. Similarly to the other cases illustrated in section 1, preliminary interpretations of these ground-surface effects are being highly controversial. Although that fault is not part of the data set analyzed here, we remark the importance of our results in providing a valuable knowledge base to interpret this phenomenon.

Acknowledgments
Supporting data are included as six supporting information files that accompany this article. The work presented in this paper was planned and funded by Project MIUR-FIRB "Abruzzo," code RBAP10ZC8K_003. We acknowledge C. Gizzi, C. Di Lorenzo, D. Di Naccio, M. Di Persio, and Gretty for their assistance with the field measurements. The thorough reviews by F.J. Pazzaglia and N. Finnegan widened the discussions and added to the overall quality of this paper. We also thank an anonymous reviewer of an earlier version of this work for his/her valuable suggestions.

References

Akinci, A., D. Perkins, A. M. Lombardi, and R. Basili (2010), Uncertainties in probability of occurrence of strong earthquakes for fault sources in the Apennines, Italy, *J. Seismol.*, *14*(1), 95–117, doi:10.1007/s10950-008-9142-y.

Alfani, G. (1915), Appunti di viaggio del padre G. Alfani sui luoghi maggiormente danneggiati dal terremoto del 13 Gennaio 1915, 14 pp., Manoscritti dell'Archivio dell'Osservatorio Ximeniano, Firenze.

Amoruso, A., L. Crescentini, A. Morelli, and R. Scarpa (2002), Slow rupture of an aseismic fault in a seismogenic region of central Italy, *Geophys. Res. Lett.*, *29*(24), 2219, doi:10.1029/2002GL016027.

Basili, R., V. Bosi, F. Galadini, P. Galli, M. Meghraoui, P. Messina, M. Moro, and A. Sposato (1998), The Colfiorito earthquake sequence of September–October 1997: Surface breaks and seismotectonic implications for the central Apennines (Italy), *J. Earthquake Eng.*, *2*, 291–302.

Benedetti, L., I. Manighetti, Y. Gaudemer, R. Finkel, J. Malavieille, K. Pou, M. Arnold, G. Aumaître, D. Bourlès, and K. Keddadouche (2013), Earthquake synchrony and clustering on Fucino faults (central Italy) as revealed from in situ ^{36}Cl exposure dating, *J. Geophys. Res.: Solid Earth*, *118*, 4948–4974, doi:10.1002/jgrb.50299.

Bianchi Fasani, G., E. Di Luzio, C. Esposito, S. G. Evans, and G. Scarascia Mugnozza (2014), Quaternary, catastrophic rock avalanches in the central Apennines (Italy): Relationships with inherited tectonic features, gravity-driven deformations and the geodynamic frame, *Geomorphology*, *211*, 22–42, doi:10.1016/j.geomorph.2013.12.027.

Bosi, C. (1975), Osservazioni preliminari su faglie probabilmente attive nell'Appennino centrale, *Boll. Soc. Geol. It.*, *94*, 827–859.

Bosi, C., F. Galadini, and P. Messina (1993), Neotectonic significance of bedrock fault scarps: case studies from the Lazio-Abruzzi Apennines (central Italy), *Z. Geomorph. N. F., Suppl.-Bd.*, *94*, 187–206.

Bubeck, A., M. Wilkinson, G. P. Roberts, P. A. Cowie, K. J. W. McCaffrey, R. Phillips, and P. Sammonds (2015), The tectonic geomorphology of bedrock scarps on active normal faults in the Italian Apennines mapped using combined ground penetrating radar and terrestrial laser scanning, *Geomorphology*, *237*, 38–51, doi:10.1016/j.geomorph.2014.03.011.

Cavinato, G. P., C. Carusi, M. Dall'Asta, E. Miccadei, and T. Piacentini (2002), Sedimentary and tectonic evolution of Plio–Pleistocene alluvial and lacustrine deposits of Fucino Basin (central Italy), *Sediment. Geol.*, *148*, 29–59.

Cello, G., G. Deiana, P. Mangano, S. Mazzoli, E. Tondi, L. Ferreli, L. Maschio, A. M. Michetti, L. Serva, and E. Vittori (1998), Evidence for surface faulting during the September 26, 1997, Colfiorito (central Italy) earthquakes, *J. Earthquake Eng.*, *2*, 303–324.

Chang, K.-T., L. Ge, and H.-H. Lin (2014), Slope creep behavior: Observations and simulations, *Environ. Earth Sci.*, *73*(1), 275–287, doi:10.1007/s12665-014-3423-2.

Cinti, F. R., D. Pantosti, P. M. De Martini, S. Pucci, R. Civico, S. Pierdominici, L. Cucci, C. A. Brunori, S. Pinzi, and A. Patera (2011), Evidence for surface faulting events along the Paganica fault prior to the 6 April 2009 L'Aquila earthquake (central Italy), *J. Geophys. Res.*, *116*, B07308, doi:10.1029/2010JB007988.

Cinti, G., A. Donati, and G. Scarascia Mugnozza (2001), La grande frana di Monte Arezzo (Abruzzo), *Mem. Soc. Geol. Ital.*, *56*, 41–50.

Cirella, A., A. Piatanesi, E. Tinti, M. Chini, and M. Cocco (2012), Complexity of the rupture process during the 2009 L'Aquila, Italy, earthquake, *Geophys. J. Int.*, *190*(1), 607–621, doi:10.1111/j.1365-246X.2012.05505.x.

Della Seta, M., C. Esposito, G. M. Marmoni, S. Martino, G. Scarascia Mugnozza, and F. Troiani (2016), Morpho-structural evolution of the valley-slope systems and related implications on slope-scale gravitational processes: New results from the Mt. Genzana case history (central Apennines, Italy), *Geomorphology*, doi:10.1016/j.geomorph.2016.07.003.

Densmore, A. L., M. A. Ellis, and R. S. Anderson (1998), Landsliding and the evolution of normal-fault-bounded mountains, *J. Geophys. Res.*, *103*, 15,203, doi:10.1029/98JB00510.

Di Luzio, E., G. Bianchi-Fasani, C. Esposito, M. Saroli, G. P. Cavinato, and G. Scarascia-Mugnozza (2003), Massive rock-slope failure in the central Apennines (Italy): The case of the Campo di Giove rock avalanche, *Bull. Eng. Geol. Environ.*, *63*(1), 1–12, doi:10.1007/s10064-003-0212-7.

Discenza, M. E., C. Esposito, S. Martino, M. Petitta, A. Prestininzi, and G. Scarascia Mugnozza (2011), The gravitational slope deformation of Mt. Rocchetta ridge (central Apennines, Italy): Geological-evolutionary model and numerical analysis, *Bull. Eng. Geol. Environ.*, *70*(4), 559–575, doi:10.1007/s10064-010-0342-7.

Elter, P., G. Giglia, M. Tongiorgi, and L. Trevisan (1975), Tensional and compressional areas in the recent (Tortonian to Present) evolution of the northern Apennines, *Boll. Geofis. Teor. Appl.*, *65*, 3–18.

Field, E. H., et al. (2013),Uniform California Earthquake Rupture Forecast, version 3 (UCERF3)—The time-independent model., U.S. Geological Survey Open-File Report 2013–1165, California Geological Survey Special Report 228, and Southern California Earthquake Center Publication 1792, http://pubs.usgs.gov/of/2013/1165/ ed., 97 pp.

Finnegan, N. J., R. Schumer, and S. Finnegan (2014), A signature of transience in bedrock river incision rates over timescales of 10(4)–10(7) years, *Nature*, *505*(7483), 391–394, doi:10.1038/nature12913.

Galli, P., P. Messina, B. Giaccio, E. Peronace, and B. Quadrio (2012), Early Pleistocene to late Holocene activity of the Magnola fault (Fucino fault system, central Italy), *Boll. Geofis. Teor. Appl.*, *53*(4), 435–458, doi:10.4430/bgta0054.

Ganti, V., K. M. Straub, E. Foufoula-Georgiou, and C. Paola (2011), Space-time dynamics of depositional systems: Experimental evidence and theoretical modeling of heavy-tailed statistics, *J. Geophys. Res.*, *116*, F02011, doi:10.1029/2010JF001893.

Gardner, T. W., D. W. Jorgensen, C. Shuman, and C. R. Lemieux (1987), Geomorphic and tectonic process rates: Effects of measured time interval, *Geology*, *15*, 259–261, doi:10.1130/0091-7613(1987)15<259:GATPRE>2.0.CO;2.

GE.MI.NA (1963), Ligniti e torbe dell'Italia continentale, 319 pp., ILTE.

Giaccio, B., F. Galadini, A. Sposato, P. Messina, M. Moro, M. Zreda, A. Cittadini, S. Salvi, and A. Todero (2002), Image processing and roughness analysis of exposed bedrock fault planes as a tool for paleoseismological analysis: Results from the Campo Felice fault (central Apennines, Italy), *Geomorphology*, *49*, 281–301.

Hiemer, S., J. Woessner, R. Basili, L. Danciu, D. Giardini, and S. Wiemer (2014), A smoothed stochastic earthquake rate model considering seismicity and fault moment release for Europe, *Geophys. J. Int.*, *198*, 1159–1172, doi:10.1093/gji/ggu186.

Improta, L., et al. (2012), High-resolution controlled-source seismic tomography across the Middle Aterno basin in the epicentral area of the 2009, M_w 6.3, L'Aquila earthquake (central Apennines, Italy), *Ital. J. Geosci.*, *131*(3), 373–388, doi:10.3301/IJG.2011.35.

Kastelic, V., M. M. C. Carafa, and F. Visini (2016), Neotectonic deformation models for probabilistic seismic hazard: A study in the external dinarides, *Geophys. J. Int.*, doi:10.1093/gji/ggw106.

Lavecchia, G., F. Ferrarini, F. Brozzetti, R. De Nardis, P. Boncio, and L. Chiaraluce (2012), From surface geology to aftershock analysis: Constraints on the geometry of the L'Aquila 2009 seismogenic fault system, *Ital. J. Geosci.*, *131*(3), 330–347, doi:10.3301/IJG.2012.24.

Mensing, S. A., et al. (2015), 2700 years of Mediterranean environmental change in central Italy: A synthesis of sedimentary and cultural records to interpret past impacts of climate on society, *Quat. Sci. Rev.*, *116*, 72–94, doi:10.1016/j.quascirev.2015.03.022.

Morewood, N. C., and G. P. Roberts (2000), The geometry, kinematics and rates of deformation within an en échelon normal fault segment boundary, central Italy, *J. Struct. Geol.*, *22*, 1027–1047.

Moro, M., M. Saroli, C. Tolomei, and S. Salvi (2009), Insights on the kinematics of deep-seated gravitational slope deformations along the 1915 Avezzano earthquake fault (central Italy), from time-series DInSAR, *Geomorphology*, *112*(3–4), 261–276, doi:10.1016/j.geomorph.2009.06.011.

Nicoletti, P. G., M. Parise, and E. Miccadei (1993), The Scanno rock avalanche (Abruzzi, south-central Italy), *Boll. Soc. Geol. Ital.*, *112*, 523–535.

Oddone, E. (1915), Gli elementi fisici del grande terremoto marsicano-fucense del 13 gennaio 1915, *Boll. Soc. Sismol. Ital.*, *19*, 71–216.

Pelletier, J. D., and C. Rasmussen (2009), Quantifying the climatic and tectonic controls on hillslope steepness and erosion rate, *Lithosphere*, *1*(2), 73–80, doi:10.1130/l3.1.

Petersen, M. D., A. D. Frankel, S. C. Harmsen, C. S. Mueller, O. S. Boyd, N. Luco, R. L. Wheeler, K. S. Rukstales, and K. M. Haller (2013), The 2008 U. S. Geological Survey national seismic hazard models and maps for the Central and eastern United States, *Geolog. Soc. Am. Spec. Pap.*, *493*, 243–257, doi:10.1130/2012.2493(12).

Piccardi, L., Y. Gaudemer, P. Tapponier, and M. Boccaletti (1999), Active oblique extension in the central Apennines (Italy): Evidence from the Fucino region, *Geophys. J. Int.*, *139*, 499–530.

Roberts, G. P., and A. M. Michetti (2004), Spatial and temporal variations in growth rates along active normal fault systems: An example from the Lazio–Abruzzo Apennines, central Italy, *J. Struct. Geol.*, *26*(2), 339–376, doi:10.1016/s0191-8141(03)00103-2.

Sadler, P. M. (1981), Sediment accumulation rates and the completeness of stratigraphic sections, *J. Geol.*, *89*(5), 569–584, doi:10.1086/628623.

Sadori, L., S. Jahns, and O. Peyron (2011), Mid-Holocene vegetation history of the central Mediterranean, *Holocene*, *21*(1), 117–129, doi:10.1177/0959683610377530.

Scarascia Mugnozza, G., G. Bianchi Fasani, C. Esposito, S. Martino, M. Saroli, E. Di Luzio, and S. G. Evans (2006), Rock avalanche and mountain slope deformation in a convex dip-slope: The case of the Maiella massif, central Italy, in *Massive Rock Slope Failure*, edited by S. G. Evans et al., pp. 357–376, NATO Science Series. Kluwer, Dordrecht.

Schlagenhauf, A. (2009), Identication des forts séismes passés sur les failles normales actives de la région Lazio-Abruzzo (Italie Centrale) par `datations cosmogéniques' (^{36}Cl) de leurs escarpements, Université Joseph-Fourier, Grenoble I, 2009. French. <tel-00461004>.

Schlagenhauf, A., Y. Gaudemer, L. Benedetti, I. Manighetti, L. Palumbo, I. Schimmelpfennig, R. Finkel, and K. Pou (2010), Using in situ chlorine-36 cosmonuclide to recover past earthquake histories on limestone normal fault scarps: A reappraisal of methodology and interpretations, *Geophys. J. Int.*, *182*, 36–72, doi:10.1111/j.1365-246X.2010.04622.x.

Schlagenhauf, A., I. Manighetti, L. Benedetti, Y. Gaudemer, R. Finkel, J. Malavieille, and K. Pou (2011), Earthquake supercycles in central Italy, inferred from ^{36}Cl exposure dating, *Earth Planet. Sci. Lett.*, *307*(3–4), 487–500, doi:10.1016/j.epsl.2011.05.022.

Schumer, R., D. Jerolmack, and B. McElroy (2011), The stratigraphic filter and bias in measurement of geologic rates, *Geophys. Res. Lett.*, *38*, L11405, 10.1029/2011GL047118.

Schumer, R., and D. J. Jerolmack (2009), Real and apparent changes in sediment deposition rates through time, *J. Geophys. Res.*, *114*, F00A06, doi:10.1029/2009JF001266.

Selby, M. J. (1993), *Hillslope Materials and Processes*, 2nd ed., pp. 451, Oxford Univ. Press, Oxford.

Serva, L., A. M. Blumetti, and A. M. Michetti (1986), Gli effetti sul terreno del terremoto del Fucino (13 gennaio 1915); tentativo di interpretazione della evoluzione tettonica recente di alcune strutture, *Mem. Soc. Geol. It.*, *35*, 893–907.

Stirling, M., et al. (2012), National seismic hazard model for New Zealand: 2010 update, *Bull. Seismol. Soc. Am.*, *102*(4), 1514–1542, doi:10.1785/0120110170.

Tesson, J., B. Pace, L. Benedetti, F. Visini, M. Delli Rocioli, M. Arnold, G. Aumaître, D. L. Bourlès, and K. Keddadouche (2016), Seismic slip history of the Pizzalto fault (central Apennines, Italy) using in situ-produced ^{36}Cl cosmic ray exposure dating and rare earth element concentrations, *J. Geophys. Res.: Solid Earth*, *121*, 1983–2003, doi:10.1002/2015jb012565.

Trigila, A., C. Iadanza, C. Esposito, and G. Scarascia-Mugnozza (2015), Comparison of Logistic Regression and Random Forests techniques for shallow landslide susceptibility assessment in Giampilieri (NE Sicily, Italy), *Geomorphology*, *249*, 119–136, doi:10.1016/j.geomorph.2015.06.001.

Trigila, A., C. Iadanza, and D. Spizzichino (2010), Quality assessment of the Italian Landslide Inventory using GIS processing, *Landslides*, *7*(4), 455–470, doi:10.1007/s10346-010-0213-0.

Valoroso, L., L. Chiaraluce, D. Piccinini, R. Di Stefano, D. Schaff, and F. Waldhauser (2013), Radiography of a normal fault system by 64,000 high-precision earthquake locations: The 2009L'Aquila (central Italy) case study, *J. Geophys. Res.: Solid Earth*, *118*, 1156–1176, doi:10.1002/jgrb.50130.

Woessner, J., et al. (2015), The 2013 European Seismic Hazard Model: Key components and results, *Bull. Earthquake Eng.*, *13*(12), 3553–3596, doi:10.1007/s10518-015-9795-1.